J Solid State Electrochem (2010) 14:1555–1563
DOI 10.1007/s10008-009-0972-5

ORIGINAL PAPER

# Pt–Ru-supported electrodes deposited by multiple successive cycles of potentiostatic pulses: evaluation of Nafion film effect on methanol oxidation

**Juan Manuel Sieben · Marta M. E. Duarte · Carlos E. Mayer**

Received: 30 September 2008 / Revised: 2 November 2009 / Accepted: 4 November 2009 / Published online: 16 December 2009


**Abstract** The influence of thin Nafion films on electrodeposited Pt–Ru electrocatalysts for the electro-oxidation of methanol was studied. Nanostructured planar carbon-supported Pt–Ru electrodes, on which a layer of Nafion ionomer was incorporated, were prepared by multiple cycles of potentiostatic pulses. SEM and AFM images of the deposit showed Pt–Ru particles grouped in agglomerates with sizes between 50 and 200 nm constituted by small nano-sized crystallites. The activity of the electrodes was found to decrease when the thickness of the Nafion film was increased, but the Tafel slope value was found to remain almost unchanged in all electrodes. These results may be associated with the partial blocking of the surface active sites by hydrophobic domains of the polymer, and the presence of $CO_2$ molecules retained within the Nafion hydrophilic microchannels.

**Keywords** Electrodeposition · Pt–Ru-supported catalyst · Nafion · Methanol oxidation

## Introduction

Direct methanol fuel cell (DMFC) is a promising conversion energy system for transport and portable applications. However, there are several serious technological challenges such as slow kinetics of methanol oxidation reaction, high cost of catalysts [1, 2] and methanol crossover to the cathode [3] that must be overcome before general application. Thermodynamically, methanol oxidation has a low equilibrium potential, but it requires a large overpotential to proceed, depending on the catalyst and operating conditions. Complete methanol oxidation requires the transference of six electrons per molecule, resulting in sluggish kinetics even on the most effective catalysts.

Pt–Ru solid solutions are considered the best catalysts for methanol electro-oxidation. Typical manufacturing methods of anodes for DMFCs involve painting, spraying, or printing of catalyst inks that contain a matrix of electrolyte phase and carbon-supported catalysts. In these methods, the utilization of the noble metal is inefficient, due to agglomeration of the catalyst powders and lack of contact between the Pt–Ru particles and the polymeric electrolyte [3].

One approach to avoid these difficulties is to prepare Pt–Ru electrodes by electrodeposition at carbon substrates in an aqueous solution. Selective deposition of catalyst particles at desirable locations in the electrode with both ionic and electronic accessibility is achieved.

One aspect that must be taken into account is the effect of the ionomer that acts as a proton conductor and a binder [4–6]. In proton exchange membranes fuel cells, Nafion commercial perfluorinated ionic polymers are the most used due to its excellent proton conductivity, thermal and chemical stability, and mechanical strength [7].

The use of planar nanostructured electrodes provides a useful tool for studying the reactions at a catalyst on which a thin layer of a polymeric conductive electrolyte has been placed. These electrodes are composed of a nanostructured catalyst electrodeposited on a non-porous conductive

J. M. Sieben (✉)
Instituto de Ingeniería Electroquímica y Corrosión (INIEC),
Universidad Nacional del Sur,
Av. Alem 1253. (B8000CPB),
Bahía Blanca, Argentina
e-mail: jmsieben@uns.edu.ar

M. M. E. Duarte · C. E. Mayer
Comisión de Investigaciones Científicas
de la Provincia de Buenos Aires (CIC),
Bahía Blanca, Buenos Aires, Argentina

substrate. With this arrangement, the effect of a porous structure is avoided although retaining the characteristics of a dispersed catalyst. This is a convenient approach to the investigation of methanol oxidation at the interface between a real electrocatalyst and a solid polymer electrolyte membrane.

The aim of the present work is to prepare planar-supported Pt–Ru electrodes by multiple successive cycles of potentiostatic pulses to study the effect of Nafion films deposited over the catalyst. Methanol electro-oxidation is examined by diverse electrochemical techniques.

## Experimental

Glassy carbon (GC) discs of 0.07 $cm^2$ exposed geometric area were used as catalyst support. Previously to Pt–Ru electrodeposition, the GC electrodes were polished with emery paper (grit 1200) and alumina of grade 1 and 0.3 μm.

Nafion® 117 films of diverse thickness were prepared dropping different amounts of a 5% alcohol solution (5 at.%, Fluka) of the ionomeric membrane over Pt–Ru/GC electrodes, followed by drying in air for a day before use. The characteristics of the different Nafion films are listed in Table 1.

Electrochemical measurements were carried out in a conventional three-compartment glass cell at temperatures between 25 and 60ºC. The counter-electrode was a platinum foil, separated from the working electrode compartment by a porous glass diaphragm. A saturated calomel electrode (+0.241 V vs. NHE) located in a Luggin capillary served as the reference electrode. All potentials mentioned in this work are referred to this electrode. An inert nitrogen atmosphere was maintained over the electrolyte. A PAR 273 potentiostat was used to run the experiments. Electrochemical techniques such as cyclic voltammetry, linear sweep voltammetry, and chronoamperometry were used to characterize the catalysts and evaluate their activities for methanol oxidation.

The catalysts were synthesized by electrodeposition at room temperature using a diluted solution of platinum and ruthenium salts (2 mM $H_2PtCl_6$+2 mM $RuCl_3$ in 0.5 M $H_2SO_4$). The electrodeposition was carried out using multiple successive potentiostatic pulses ($E_{cathodic}$=−0.5 V $t_{cathodic}$=30 s, $E_{anodic}$=1 V $t_{anodic}$=5 s). All electrodes were prepared by applying 30 consecutive cycles. After deposition, the electrodes were thoroughly rinsed with bidistilled water and tested in sulfuric acid solution by cyclic voltammetry at a rate of 50 mV $s^{-1}$ to evaluate reproducibility. The catalyst active surface area has been found to depend positively on the number of cathodic potential pulses at −0.5 V, and on the potential of the anodic pulse. At −0.5 V a large quantity of nuclei are formed, whereas the effect of the positive pulse at 1.0 V is the rapid oxidation of the hydrogen formed during the negative pulse, facilitating the formation of new nuclei [8].

**Table 1** Characteristics of Nafion layer

| $V_{Nafion}$/μL | $W/A_g$ mg $cm^{-2}$ | $l_{dry}$/μm |
|---|---|---|
| 1 | 0.621 | 0.85±0.30 |
| 5 | 3.107 | 5.10±0.40 |
| 10 | 6.214 | 9.72±0.43 |

$W$ weight of Nafion film, $l_{dry}$ thickness of dry Nafion film measured by SEM microscopy, $A_g$ geometric area

The active surface area of the electrocatalysts was determined by copper underpotential deposition. Experimental details were described in a previous paper [9]. The average active surface area of the electrocatalysts was 34.86±0.03 $cm^{-2}$ per unit of geometric area.

The electrode activity for methanol oxidation was measured in 1 M $CH_3OH$+0.5 M $H_2SO_4$ solution by cyclic voltammetry at a scan rate of 50 mV $s^{-1}$, starting at 0 V. Chronoamperometry curves were obtained at different potentials, applying potential pulses from an initial potential of 0 V. Current densities are referred to the active surface area before Nafion deposition.

The morphology of the catalyst surface and the particle size were analyzed using scanning electronic microscopy (SEM; JEOL 100) and atomic force microscopy in non-contact mode (AFM; Nanoscope Digitals Instruments). Bulk composition analysis of Pt–Ru catalysts was performed using an X-ray detector for energy dispersive spectroscopy analysis (SEM-EDX). In addition, the structure of the electrodes was characterized by X-ray diffraction (XRD) using a Rigaku Dmax III C diffractometer with monochromated CuKα radiation.

The catalyst loading for some selected electrodes was determined by dissolution in aqua regia and posterior analysis by ICP-AES (Shimadzu 1000 model III analyzer). Under these conditions, metal loadings of 0.30± 0.05 mg $cm^{-2}$ were measured.

## Results and discussion

### Characterization of the Pt–Ru/GC and Nafion/Pt–Ru/GC systems

The atomic composition of Pt–Ru catalysts was determined by EDX technique. Ru contents between 23 and 25 wt.% were measured in all the analyzed samples. The proportion of deposited ruthenium to platinum is within the expected order, taking into account that the mol ratio of $RuCl_3$ concentration to $H_2PtCl_6$ concentration is equal to one [9]. It is possible that the existence of adsorbed hydrogen on the platinum surface blocked metal ion access to the electrode

surface inhibiting metal deposition. Moreover, it is known that in the case of a smooth ruthenium layer, the ionization of hydrogen at −0.2 V is accompanied by adsorption of water on ruthenium atoms and this process might influence metal deposition [10–12].

A SEM micrograph of Pt–Ru catalyst on glassy carbon is shown in Fig. 1a, while the SEM image in Fig. 1b shows that the surface of the ionomer film is flat and smooth in microscale.

Electrodeposited platinum particles generally exhibit uniform size and semispherical shape and appear regularly distributed over the support surface [13]. However, the electrodeposition method here used generates rough islands with incipient dendritic structure. The formation of dendrites occurs in the mass-transfer or mixed control regions [14], and under this condition, the particle growth is accelerated due to a faster diffusion rate of the metal ions at the tips of the excrescences [15]. Another plausible explanation suggests that crystallite tips formation is probably a consequence of the interaction between primary and secondary nucleation, where the depletion zone formed around the metallic nuclei at high overpotential promotes secondary nuclei growth, resulting in the formation of ramified structures [16]. Ruthenium codeposition does not modify the morphology appreciably, but an increase in particle size is observed [9]. Although the particles tend to coalesce and to overlap one with the other, the existence of smaller particles suggests that new nuclei are formed throughout all the process.

The AFM image in Fig. 2a gives a top view of the catalyst deposited on the GC substrate. The metal particles may be envisaged as packed piles of nanoscale clusters forming a kind of grouped lamellar agglomerates (Fig 2b) with sizes between 50 to 200 nm, in concordance with those determined from SEM images. Similar particle morphology was observed by Paoletti et al. [17] on carbon-supported Pt catalysts prepared by multiple galvanostatic pulsed electrodeposition. In addition, the formation of secondary nuclei is also observed (Fig. 2a).

It is known that electrodeposition of noble metals on carbon supports occurs via 3D nucleation and growth mechanism [18]. Generally, primary nucleation on carbon is followed by secondary nucleation on predeposited Pt surface, except when short potential pulses are employed [19]. This behavior may be explained considering that a higher concentration of nucleation centers on Pt surface compared with carbon [20]. The result of secondary nucleation is the formation of complex micro- and nano-grained Pt structures [16, 20]. Furthermore, on atomically smooth highly orientated pyrolytic graphite (HOPG) surface formation of particle agglomerates may also occur through migration and coalescence of Pt nanoparticles favored by weak interaction of Pt with HOPG substrate. Therefore, Gloaguen et al. [18] and Zoval et al. [19] concluded that Pt electrodeposition on HOPG takes place via formation of particles 10–20 nm in diameter and their surface diffusion sticking, which results in agglomeration. In fact, both secondary nucleation and surface diffusion sticking can contribute to the catalyst morphology observed in SEM and AFM images.

XRD spectra reveal the bulk structure of the catalyst and its support (Fig. 3). The diffraction peaks referred to carbon support are located at $2\theta$ values of about 25°, 42°, and 54° in the XRD spectra. The diffractograms show three peaks characteristic of face-centered cubic (fcc) crystalline at approximately $2\theta$ values of 40.1°, 47.3°, and 68.5°, which are associated with the (111), (200), and (220) planes, respectively, indicating that the catalysts have principally single-phase disordered structure (i.e., solid solutions). Comparing with the reflections of pure Pt, the diffraction peaks for the Pt–Ru catalysts are shifted slightly toward higher $2\theta$ values. The slight shift of the diffraction peaks reveals the formation of an alloy involving the incorporation of Ru atoms into the fcc structure of Pt. It is important to note that no diffraction peaks indicate the presence of either pure Ru or Ru-rich hexagonal close packed phase.

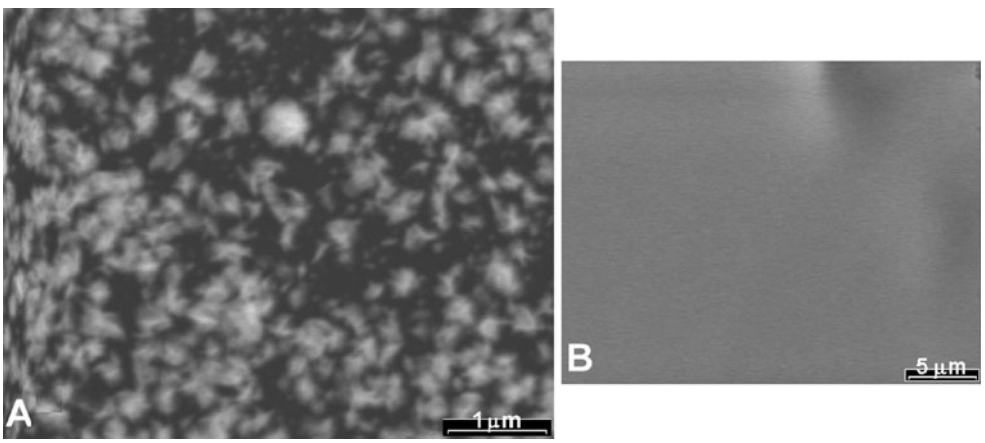


**Fig. 1** SEM image of a Pt–Ru/GC electrode (**a**). SEM image showing a Nafion film over a supported Pt–Ru catalyst (**b**). The catalyst was prepared at the following conditions: $E_{cathodic}$=−0.5 V, $t_{cathodic}$=30 s; $E_{anodic}$=1 V, $t_{anodic}$=5 s; 30 cycles

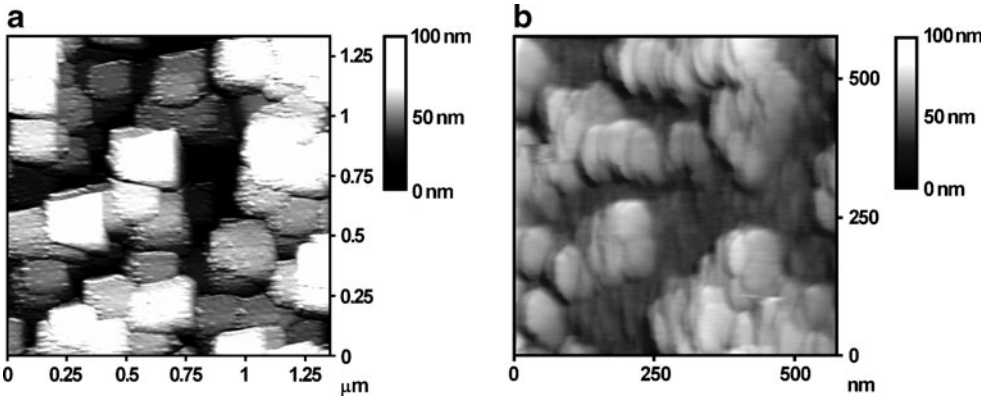


**Fig. 2** AFM images of a Pt–Ru/GC electrode. The catalyst was prepared at the following conditions: $E_{cathodic}$=−0.5 V, $t_{cathodic}$=30 s; $E_{anodic}$=1 V, $t_{anodic}$=5 s; 30 cycles

The peak profiles in XRD patterns of the catalysts were obtained by integration of the respective areas after peak deconvolution using the Marquardt algorithm. A lattice constant of 3.922±0.004 Å was determined for Pt/GC in good agreement with 3.923 Å for pure Pt, whereas a value of 3.892±0.005 Å was obtained for Pt–Ru/GC. In accordance with the Vegards' law, the nominal Ru content of the Pt–Ru catalyst was around 25%, agreeing with EDX results.

Debye–Scherrer's equation was used to estimate the average Pt–Ru crystallite size from the most distinct peak, Pt (111) centered around $2\theta$ =40.2°. The average size of the crystallite was found to be around 5 nm, in accordance with the sizes obtained by Coutanceau et al. [21] with electrodes prepared by galvanostatic pulsed electrodeposition.

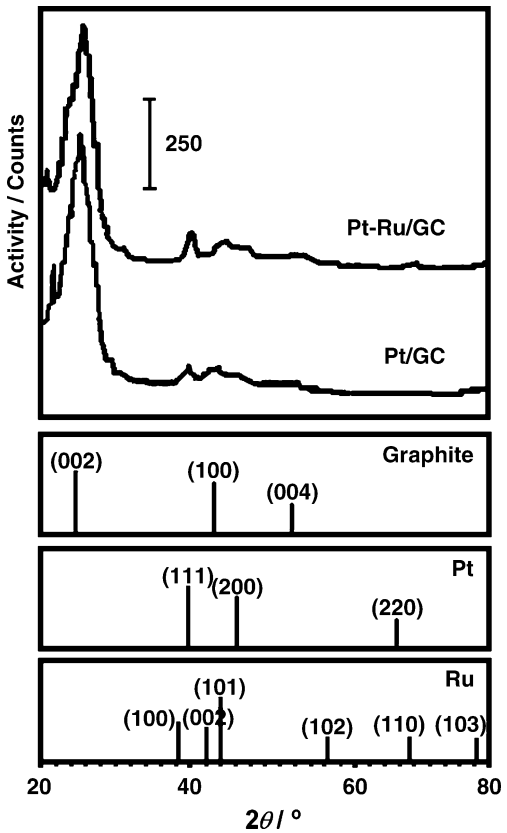


**Fig. 3** XRD patterns of Pt/GC and Pt–Ru/GC electrodes. Platinum and ruthenium were deposited at the following conditions: $E_{cathodic}$=−0.5 V, $t_{cathodic}$=30 s; $E_{anodic}$=1 V, $t_{anodic}$=5 s; 30 cycles

The specific surface area of the metal ($S_w$/m$^2$ g$^{-1}$), in the absence of any screening or coalescence of crystals, can be estimated from the mean particle size determined by XRD:

$$S_w = \frac{6 \times 10^4}{\rho\, d} \tag{1}$$

The catalyst density $\rho$ can be calculated by two different ways, using the lattice parameter or the pure metal's density. Both methods give similar results. Using the lattice parameter, we have:

$$\rho = \frac{\text{Unit cell weight}}{\text{Unit cell volume}} = 4x10^{24}\left[\frac{X_{Pt}M_{Pt} + X_{Ru}M_{Ru}}{a_{fcc}^3 N_A}\right] \tag{2}$$

where $\rho$ (g cm$^{-3}$) is the density of Pt–Ru alloy, $X_{Pt}$ and $X_{Ru}$ are the atomic fractions of Pt and Ru, $M_{Pt}$, and $M_{Ru}$ are the molecular weights (g mol$^{-1}$), $a_{fcc}$ (Å) is the lattice parameter and $N_A$ is the Avogadro number. Using Eq. 1, specific surface area values of around 65 m$^2$ g$^{-1}$ and 35 m$^2$ g$^{-1}$ are estimated for Pt–Ru and Pt catalysts, respectively. Therefore, the specific surface area of this bimetallic alloy is significantly larger than the platinum catalyst surface area, probably due to the decrease of both alloy density and crystallite size.

It should be noted that the specific surface area estimated from XRD considerably exceeds the value obtained from Cu stripping and ICP analysis. This behavior can be explained by particle agglomeration at the experimental conditions used to prepare the catalysts. The degree of particle coalescence $\xi$ [22] can be calculated with Eq. 3:

$$\xi = 1 - \frac{S_{w,\,EC}}{S_{w,\,calc}} \tag{3}$$

Here $S_{w,\,EC}$ is the specific surface area determined from Cu stripping and ICP analysis and $S_{w,\,calc}$ is the specific surface area calculated from the results of XRD. The

calculation gives a $\xi$ value of about 0.9, indicating high degree of particle agglomeration. Therefore, part of the nano-sized particle surface will be scarcely accessible to the solution, explaining the lower value of surface area determined by Cu stripping.

Cyclic voltammograms of Nafion/Pt–Ru electrodes with variable ionomer thickness are shown in Fig. 4. In sulphuric acid solution, well-defined hydrogen-associated faradic processes are observed. Nevertheless, the coulombic charge related to the hydrogen adsorption/desorption processes decreases when Nafion film thickness increases. A difference of about 23% between charges under the peaks for the electrodes without Nafion and with the thinnest polymeric film was determined. In addition, charges reduction of 57% and 62% were found for Nafion films with thicknesses of 5.10 and 9.72 μm, respectively. The amorphous part of the perfluorocarbon backbone can partially block the electrochemical active sites in the catalyst surface by the formation of hydrophobic domains that hinder the proton access to the electrode surface. This blocking is consistent with the effect observed on a smooth polycrystalline platinum electrode [23, 24]. In addition, when the electrode is covered by the polymeric film the extent to which the ionomer penetrates the mesoporous structure of the supported catalyst is unknown. The wetting of the electrode mesoporous structure by the Nafion solution is deficient, so the incomplete penetration (compared with the bare electrode) might also contribute to decrease hydrogen adsorption on Pt atoms.

## Methanol oxidation

Figure 5 shows the cyclic voltammetry curves recorded for the different Nafion/Pt–Ru/GC electrodes at temperatures between 25 and 60ºC at 50 mV $s^{-1}$. The onset of methanol oxidation takes place at 0.35 V at 25ºC and shift to lower potentials with increasing temperature, falling to 0.2 V at 60ºC. The lower onset for methanol oxidation and the increase in catalytic activity at higher temperatures is a consequence of the high rate constant of the oxidation reaction. In addition, the electrode performance for methanol oxidation, taken from the current peak, increases more than ten times when the temperature is raised from 25 to 60°C.

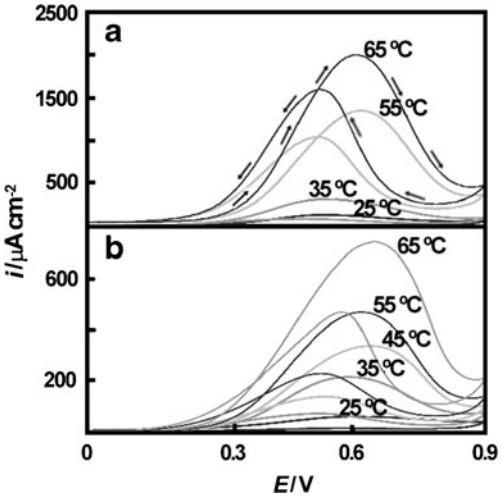


**Fig. 5** Cyclic voltammograms for Nafion/Pt–Ru/GC in 1 M $CH_3OH$/0.5 M $H_2SO_4$ (sweep rate 50 mV $s^{-1}$) at diverse temperatures for Nafion films of different thickness: 0.85 μm (**a**), 9.72 μm (**b**)

This behavior cannot be attributed only to an increased coverage of active surface oxidized species. The desorption rate of the adsorbed residues increases with temperature because the adsorption energy decreases, resulting in weakly adsorbed and more reactive $CO_{ads}$ molecules. In addition, the methanol diffusion rate, which has an activation energy of the order of 20 kJ $mol^{-1}$ [25], increases with temperature.

The potential of the peak that is observed in the anodic scan is shifted slightly negatively with increasing temperature, whereas the peak that appears during the cathodic scan suffers a slight positive shift. This behavior can be reasonable explained if the coverage of OH adsorbed

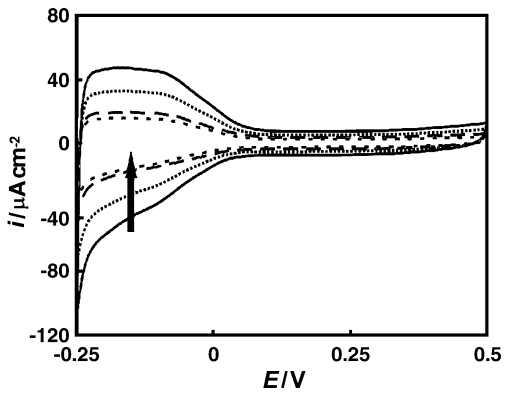


**Fig. 4** Cyclic voltammograms for Nafion/Pt–Ru/GC in 0.5 M $H_2SO_4$. Nafion film thickness: without ionomer (▬), 0.85 μm (▪▪▪), 5.10 μm (▬ ▬), and 9.72 μm (▪ ▪). Sweep rate 50 mV $s^{-1}$

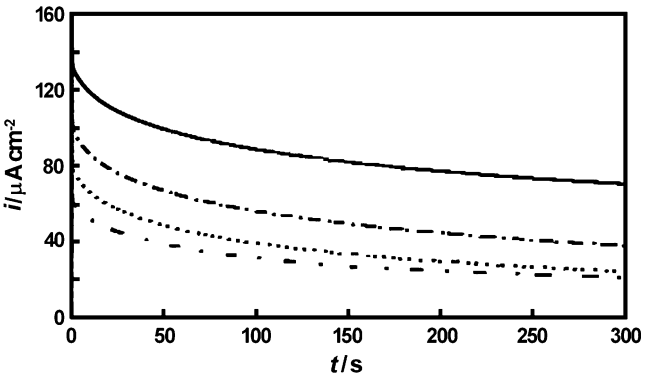


**Fig. 6** Chronoamperometry curves at 0.3 V for Nafion/Pt–Ru/GC in 1 M $CH_3OH$/0.5 M $H_2SO_4$ at room temperature. Nafion film thickness: without ionomer (▬), 0.85 μm (▪▪▪), 5.10 μm (▪▪▪), and 9.72 μm (▪ ▬)

**Table 2** Steady-state catalytic activities of methanol oxidation on electrodeposited bimetallic Pt–Ru/GC as synthesized in this work and some catalysts prepared by different deposition techniques

| Pt–Ru/C | At.% Ru | $E$/V[e] | Substrate | Precursor | Deposition method/Alcohol solution | $i$/μA cm$^{-2}$ | | | | | |
|---|---|---|---|---|---|---|---|---|---|---|---|
| | | | | | | 25 °C | 35 °C | 45 °C | 55 °C | 60 °C | 65 °C |
| Without Nafion | 25 | 0.3 | GC | $H_2PtCl_6$, $RuCl_3$ | See Experimental section. 1 M $CH_3OH$+0.5 M $H_2SO_4$ | 71.6 | 174.6 | 220.1 | 342.7 | – | 490.9 |
| 0.85 μm | | | | | | 44.7 | 116.7 | 145.3 | 223.6 | – | 325.0 |
| 5.10 μm | | | | | | 29.4 | 71.5 | 85.4 | 111.8 | – | 141.7 |
| 9.72 μm | | | | | | 26.2 | 67.3 | 80.6 | 105.1 | – | 131.8 |
| [29] | 12 | 0.5 | HOPG | $K_2PtCl_6$, $RuCl_3$ | Cyclic voltammetry sequential Pt and Ru deposition | 52 | | | | | |
| | 10 | | | | Cyclic voltammetry. simultaneous Pt and Ru deposition. 1 M $CH_3OH$+0.5 M $H_2SO_4$ | 27 | | | | | |
| [30] | | 0.25 | Carbon[d] black | $Pt(NH_3)_2(NO_2)_2$+ | Coimpregnation method, EtOH/$H_2$. | | | | | | |
| | 50 | | | $Ru_3(CO)_{12}$ | Pyrolysis temperature 200 °C | | | | | 160 | |
| | 50 | | | $RuNO(NO_3)_x$ | 1 M $CH_3OH$+0.5 M $H_2SO_4$ | | | | | 170 | |
| [31] | 40 | 0.25 | Vulcan[d] | Non identified | Colloidal method $NaHSO_3/H_2$ | 28 | | | | | |
| | 40 | | Vulcan-O[a] | | 2 M $CH_3OH$ +0.5 M $H_2SO_4$ | 75 | | | | | |
| | 50 | | Carbon[b] | | | 56 | | | | | |
| [32] | 50 | 0.3 | Vulcan | $H_2PtCl_6$, $K_2RuNOCl_5$ | Potentiostatic deposition 1 M $CH_3OH$+0.5 M $H_2SO_4$ | | | | | 158.4 | |
| [33] | 48 | 0.4 | Vulcan[d] | $H_2PtCl_6$, $RuCl_3$ | Microemulsion method. Ciclohexane/HCHO/NP5+NP9 2 M $CH_3OH$+0.5 M $H_2SO_4$ | 74 | | | | | |
| [34] | 41 | | Vulcan[d] | $H_2PtCl_6$, $RuCl_3$ | Colloidal method. $NaHSO_3/H_2O_2/H_2$ | 13 | | | | | |
| | 41 | | Vulcan-O | | 1 M $CH_3OH$+0.5 M $H_2SO_4$ | 30.5 | | | | | |
| | 44 | | Vulcan-N[c] | | Impregnation method. i-PrOH | 24 | | | | | |
| | | 0.3 | | | | | | | | | |
| | 44 | | Vulcan[d] | | | 14 | | | | | |
| | 44 | | Vulcan-O | | | 12 | | | | | |
| | 41 | | Vulcan-N | | | 16 | | | | | |

[a] Oxygen-functionalized carbon material

[b] HiSPEC 5000, Johnson and Matthey

[c] Nitrogen-functionalized carbon material

[d] Carbon black and Vulcan XC-72 supported over GC

[e] Potentials are referred to SCE electrode

species changes with temperature. Furthermore, as was mentioned, increasing temperature accelerates the chemisorption of methanol on the catalyst active sites, and increases the diffusion rate of alcohol molecules.

The presence of a Nafion film reduces the electrode activity for methanol oxidation (Figs. 5 and 6). The electrode activity when the film is absent is higher than that obtained using the electrode with the thinnest Nafion film layer. Nevertheless, the catalyst activity for methanol oxidation is similar for Nafion films with thicknesses of 5.10 and 9.72 μm. The significant decrease observed in presence of the polymeric film, can be correlated to a reduction of available active sites on the catalyst surface and the inefficiently penetration of the polymer in the catalyst structure, as was commented previously. Furthermore, the polymer presence on a planar electrode may also retard the $CO_2$ removal from the active reaction sites. In other words, $CO_2$ elimination must occur by diffusion through the membrane hydrophilic channels, becoming more difficult when Nafion film thickness increases. This can result in entrapment of the gas inside the polymeric layer and blocking of the microchannels in the structure, limiting the arrival of the reactant to the catalyst surface.

The similitude in the catalytic activity of the electrodes with Nafion thicknesses of 5.10 and 9.72 μm can be related to a similar quantity of available active sites for methanol oxidation. Besides, the existence of bigger clusters of water molecules inside the polymeric structure facilitates $CO_2$ elimination making easier the arrival of methanol to the electrode surface [26].

Chronoamperometric curves recorded in a potential range between 0.2 and 0.6 V corroborate the current decrease on both bare and Nafion covered Pt–Ru/GC electrodes. This current decay is observed in the literature for Pt–Ru catalyst at different temperatures and methanol concentrations [27, 28]. The main cause of the current decay is the blocking of the active sites by the poisoning species. Chemisorption of methanol gives rise to the adsorption of CHO and CO intermediaries with the former detected at short adsorption times and low potentials [28]. This result suggests that carbon monoxide specie acts as poison but possibly not the only one because the reaction is deactivated even at the potentials where CO is oxidized by the presence of OH species adsorbed on Ru atoms.

Electrocatalytic behavior of the electrodes prepared in this work was evaluated by potentiostatic experiments in the potential region that is relevant for methanol oxidation in DMFC and compared with some data available in the literature [29–34] (Table 2). The catalytic activities at different temperatures for the electrodes prepared here, even those covered by the polymeric film, are satisfactory when they are compared with electrodes prepared by other electrochemical techniques [29, 32], colloids formation [31, 34], impregnation [30, 34], and microemulsion methods [33]. Based on particle-size analysis alone, the activity of the homemade catalysts would be expected to be lower than that of catalysts prepared by chemical methods, due to its large average particle diameter. Perhaps the better performance of the homemade catalysts can be straightforward associated with their pronounced defective structure, i.e., high concentration of intergrain boundaries and nanopores. The presence of surface defects seems to be a *sine qua non* condition for achieving high catalytic activity as was clearly explained by Cherstiouk et al. [35], since grain boundaries can act similarly to low coordinated sites as kinks and steps, which has been identified to be highly catalytically active sites. As it was mentioned previously, surface diffusion sticking and secondary nucleation of single metal particles produces particle agglomeration and complex multi-grain structures, consisting of nanosized ordered crystalline domains interconnected by grain boundaries [22].

In addition, the ruthenium content in the solid solution and the homogeneous distribution of both metals at atomic scale can explain the behavior of the homemade catalysts [27]. It is known that a Pt–Ru alloy with low Ru content (10–20 at.%) exhibits the best performance for methanol oxidation. Higher ruthenium content reduces the available surface sites where the methanol adsorption reaction is taking place, reducing the activity of the catalysts; which can be easily explained using the statistical interpretation of bifunctional Pt–Ru electrodes suggested by Gasteiger et al. [27].

Furthermore, another reason that can be put forward to explain the lesser activity of the catalysts synthesized by chemical methods may be related to the nature of Pt–Ru species in the catalyst surface. Analyses of the catalysts by

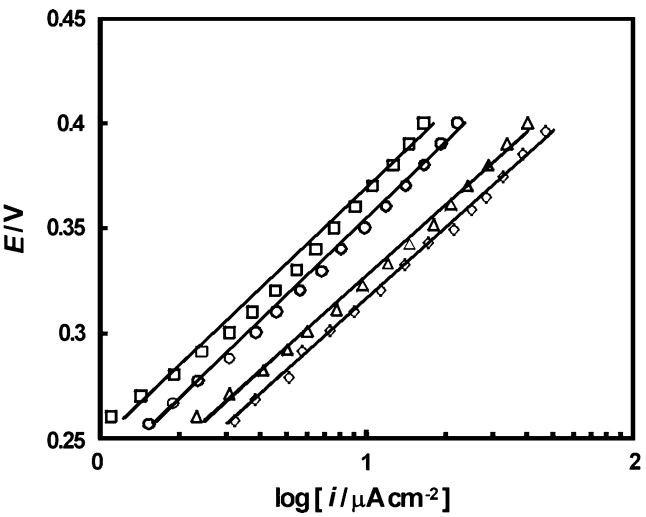


**Fig. 7** Tafel plot at 25 °C for Nafion/Pt–Ru/GC in 1 M $CH_3OH$/0.5 M $H_2SO_4$ Nafion films of different thickness: without ionomer (*empty diamond*), 0.85 μm (*empty triangle*), 5.10 μm (*empty circle*), and 9.72 μm (*empty square*)

photoelectron spectroscopy are conclusive on the presence of Pt, Pt (II), and Pt (IV) species in most of the catalysts prepared by chemical methods [34, 36]. The presence of oxidized Pt species such as PtO and $PtO_2$ in these Pt–Ru supported catalysts would contribute to their lesser activity due to a reduction of the available sites for methanol adsorption.

Figure 7 shows the Tafel plots obtained from stationary polarization experiments for methanol oxidation in 1 M $CH_3OH$+0.5 M $H_2SO_4$ solutions at room temperature for different Nafion thicknesses. The slopes were obtained in the potential region in which the studied systems obey a Tafel-type behavior. Although the linear region was not wide enough in all cases, values ranging from 115 to 125 mV $dec^{-1}$ were determined with a reasonable level of accuracy between 0.25 and 0.4 V, while in the higher potential region (>0.5 V) current maximums were observed. Tafel slopes from 105 to 130 mV $dec^{-1}$ have been reported for methanol oxidation in $HClO_4$ solution at room temperature to carbon supported Pt–Ru catalyst [37], about 110 mV $dec^{-1}$ on Johnson Mattthey catalyst (Pt/Ru atomic ratio 1:1) at 60ºC [38], 120 to 140 mV $dec^{-1}$ on electrodeposited Pt–Ru/GC (7<Ru at.% <20) between 25 and 60ºC [25], and 125 mV $dec^{-1}$ to Pt–Ru catalyst on Vulcan XC-72 at a MEA [39]. These values of Tafel slope are frequently associated with the oxidative removal or desorption of adsorbed species from the surface as the rate-determining step [9, 37].

The Tafel slope shown in Fig. 7 is ca. 120 mV $dec^{-1}$ for all the electrodes, but the lines are shifted to higher potentials (for a given current density) with increased ionomer film thickness. If the activity of the material decrease by a factor of 2–3 (see the hydrogen adsorption/desorption peaks in Fig. 4), the Tafel line should be shifted by ca. 50 mV, as it is observed in Fig. 7. This behavior confirms that, in the Tafel regime, transport issues are not a problem and the decreased activity of the electrocatalyst probably only depends on the blocking of active sites by the ionomer, as was presented in a detailed analysis by Vidaković et al. [39]. Zecevic et al. [39] observed the same behavior in oxygen reduction on a Pt electrode covered with thin films of polybenzoimidazole or Nafion. In [40] the diffusion processes begin to play a significant role at higher potentials (>0.5 V), but without reaching pure mass transfer controlled conditions.

In this way, diffusion problems can be discarded in the entire potential range studied here, although transport problems may be a limiting factor for methanol oxidation reaction at larger current densities.

## Conclusions

The dendritic structure of the Pt–Ru particles prepared by electrodeposition can be attributed to a deposition process that occurs in the mass-transfer or mixed control regions and to the interaction between primary and secondary nucleation.

The electrodes prepared by successive cycles of potentiostat pulses present a good activity for methanol oxidation, even when a polymeric film is deposited over the catalyst. The better performance of the homemade catalysts can be associated with the particle morphology, the homogeneous mixing of both metals at the atomic scale and the ruthenium content in the solid solution. However, important changes are observed when the Pt–Ru/GC electrode surface is covered by a Nafion film.

The electrochemical determinations show a decrease of the activity in the Nafion/Pt–Ru/GC electrodes with respect to the bare electrode. This behavior may be associated with two effects:

1. The partial blocking of the surface active sites by the hydrophobic domains of the polymeric film;
2. The delaying of $CO_2$ removal from the active platinum sites by the polymer, which may difficult $CH_3OH$ arrival to the catalyst surface active sites.

**Acknowledgements** This work was supported by ANPCYT grant No. 10-11133, UNS grant 24/M097 and CIC. J.M.S. is grateful to the CONICET for a postdoctoral fellowship, also J.M.S. would like to thank Dr. D. Salinas for the AFM support.

## References

1. Hogarth MP, Ralph TR (2002) Platinum Metals Rev 46:146
2. Spinace EV, Neto AO, Linardi M (2004) J Power Sources 129:121
3. Petrii O (2008) J Solid State Electrochem 12:609
4. Arico AS, Srinivasan S, Antonucci V (2001) Fuel Cells 2:133
5. Iwasita T (2003) In: Vielstich W et al (eds) Handbook of fuel cells fundamentals, technology and applications, vol. 2. Wiley, New York, p 603
6. Lamy C, Léger J-M, Srinivasan S (2001) In: Bockris JO`M, Conway BE, White RE (eds) Modern aspects of electrochemistry, vol. 34. Kluwer Academic/Plenum, New York, p 53
7. Sone Y, Ekdunge P, Simonsson D (1996) J Electrochem Soc 143:1254
8. García MF, Sieben JM, Pilla AS, Duarte MME, Mayer CE (2008) Int J Hydrogen Energy 33:3517
9. Sieben JM, Duarte MME, Mayer CE (2008) J Appl Electrochem 38:483
10. Vuković M, Čukman D (1999) J Electroanal Chem 474:167
11. Hadži-Jordanov S, Argerstein H, Vuković M, Conway BE (1977) J Phys Chem 81:2271
12. Hepel T, Pollak FH, O'Grady WE (1984) J Electrochem Soc 131:2094.
13. Hogarth MP, Punk J, Shukla AK, Hamnett A (1994) J Appl Electrochem 24:85
14. Bockris JO'M, Khan SUM (1993) Surface electrochemistry. A molecular level approach. Plenum Press, New York, p 361
15. Bard AJ, Faulkner CR (1980) Electrochemical Methods, Fundamentals and Applications, 2nd edn. Wiley, Singapore

16. Plyasova LM, Molina IY, Gavrilov AN, Cherepanova SV, Cherstiouk OV, Rudina NA, Savinova ER, Tsirlina GA (2006) Electrochim Acta 51:4477
17. Paoletti C, Cemmi A, Giorgi L, Giorgi R, Pilloni L, Serra E, Pascuali M (2008) J Power Sources 183:84
18. Gloaguen F, Léger JM, Lamy C, Marmann A, Stimming U, Vogel R (1999) Electrochim Acta 44:1805
19. Zoval JV, Lee J, Gorer S, Penner RM (1998) J Phys Chem B 102:1166
20. Cherstiouk OV, Pron'kin SN, Chuvilin AL, Salanov AN, Savinova ER, Tsirlina GA, Petrii OA (2000) Russ J Electrochem 36:741
21. Coutanceau C, Rakotondrainibe AF, Lima A, Garnier E, Pronier S, Léger J-M, Lamy C (2004) J Appl Electrochem 34:61
22. Gavrilov AN, Savinova ER, Simonov PA, Zaikovskii PI, Cherepanova SV, Tsirlina GA, Parmon VN (2007) Phys Chem Chem Phys 9:5476
23. Jiang J, Kucernak A (2004) J Electroanal Chem 567:123
24. Croissant MJ, Napporn T, Léger J-M, Lamy JM (1998) Electrochim Acta 43:2447
25. Lobato J, Cañizares P, Rodrigo MA, Linares JJ, Fernández-Fragua A (2006) Chem Eng Sci 61:4773
26. Ma S, Odgaard M, Skou E (2005) Solid State Ionics 176:2923
27. Gasteiger HA, Marković N, Ross PN Jr, Cairns E (1993) J Phys Chem 97:12020
28. Parsons R, VanderNoot T (1988) J Electroanal Chem 257:9
29. Rodríguez-Nieto FJ, Morante-Catacora TY, Cabrera CR (2004) J Electroanal Chem 571:15
30. Takasu Y, Fujiwara T, Murakami Y, Sasaki K, Oguri M, Asaki T, Sugimoto W (2000) J Electrochem Soc 147:4421
31. de la Gómez Fuente JL, Martínez-Huerta MV, Rojas S, Terreros P, Fierro JLG, Peña MA (2005) Carbon 43:3002
32. Tusseeva EK, Mikhaylova AA, Khazova OA, Kourtakis K-D (2004) Russian J Electrochem 40:1146
33. Liu Z, Ling XY, Lee JY, Su X, Gan LM (2003) J Mater Chem 13:3049
34. de la Gómez Fuente JL, Martínez-Huerta MV, Rojas S, Terreros P, Fierro JLG, Peña MA (2006) Catal Today 116:422
35. Cherstiouk OV, Gavrilov AN, Plyasova LM, Molina IY, Tsirlina GA, Savinova ER (2008) J Solid State Electrochem 12:497
36. Aricó AS, Creti P, Kim H, Mantenga R, Giordano N, Antonucci V (1996) J Electrochem Soc 143:3047
37. Gojković SL, Vidaković TR, Durović DR (2003) Electrochim Acta 48:3607
38. Vidaković T, Christov M, Sundmacher K (2005) J Electroanal Chem 580:105
39. Vidaković T, Christov M, Sundmacher K (2004) Electrochim Acta 49:2179
40. Zecevic SK, Wainright JS, Litt MH, Gojkovic SLj, Savinell RF (1997) J Electrochem Soc 144:2973